Chapter 4: RESULTS AND DISCUSSION

4.1 REHEATING EXPERIMENTAL CONDITIONS AND RESULTS

The reheating conditions, for samples prepared for scale characterisation, are summarised in Table 4.1 (a list of symbols is given from p. xiii).

TABLE 4.1*:* Reheating conditions and mass gain results

Sample	T[°C]	%O_2	mi [g]	t[h]	m_F [g]	Ss [cm^2]	e[cm]	ma[g]	Δm [g]	Gm [g/cm^2]	f_l[µm]	Cf [g/cm^2]
S6	1250	4	93.928	2	0.194	11.31	1.3	95.09	0.968	0.086	66	0.017
S7	1250	4	85.425	2	0	11.31	1.3	86.8	1.375	0.122	0	0
S8	1250	3	82.734	2	0.194	9	1.3	83.702	0.774	0.086	83	0.022
S9	1250	3	68.749	2	0	9	1.3	70.124	1.375	0.153	0	0
S10	1250	4	68.896	2	0.192	12.87	1.3	71.11	2.022	0.157	57	0.015
S11	1250	4	72.074	2	0.183	8.4	1.3	73.593	1.336	0.159	84	0.022
S12	1250	4	71.424	2	0	12.87	1.3	73.761	2.337	0.182	0	0
S13	1250	3	62.884	2	0.163	14.82	1.3	64.108	1.061	0.072	42	0.011
S14	1250	3	134.26	2	0	12.87	1.3	136.88	2.619	0.203	0	0
R 1	1250	4	184.39	5	0.28	10.925	1.55	186.21	1.54	0.141	99	0.026
RP2	1250	4	130.19	3	0	12.95	1.3	134.25	4.06	0.314	0	0
RP3	1250	4	129.05	3	0.2	12.95	1.3	131.29	2.04	0.158	59	0.015
PR4	1280	4	166.81	6	0.16	18.81	1.2	172.02	5.05	0.269	33	0.009
RP5	1280	4	188.01	6	0	21.16	1.4	194.31	6.3	0.298	0	0
RP8	1280	4	160.08	6	0.22	14.85	1.4	164.09	3.79	0.256	57	0.015
RST14	1280	4	163.87	5	0.24	15.6	1.3	166.76	2.65	0.170	59	0.015
RST13	1280	4	157.77	5	0.23	15.66	1.3	163.31	5.31	0.339	57	0.015
RST100	1280	4	180.55	5	0.3	18.18	1.3	183.6	2.75	0.151	64	0.017
RTS100	1280	4	180.02	5	0.31	18.18	1.3	183.6	3.27	0.180	66	0.017
RTS99	1280	4	178.95	5	0.325	19.825	1.15	182.36	3.085	0.156	63	0.016
RTS122	1280	4	165.44	5	0.27	16.66	1.3	170.07	4.63	0.262	62	0.016
RST10	1280	4	182.5	6	0.33	19.04	1.3	183.6	3.58	0.188	67	0.017
RTS9	1280	4	179.7	6	0.30	18.25	1.15	182.36	3.08	0.169	63	0.016
RTS12	1280	4	175.4	6	0.32	20.04	1.3	170.07	4.63	0.231	62	0.016
PR1	1250	3	170.8	2	0.08	15.43	1.2	172.02	5.05	0.327	20	0.005
R2	1250	4	135.2	6	0.163	14.76	1.3	138.41	3.05	0.206	43	0.011
R3	1250	4	132.8	6	0	12.87	1.3	137.38	4.58	0.356	0	0

X-Ray diffraction analysis for phase identification of the detached scale (after cooling in the nitrogen-flushed box) was performed on solid scale oxides (see Appendix 4**).** Surface analyses (XPS) were done to determine the chromium oxidation state (see Appendix 5). Scanning electron microscopy (SEM-BSE, SEM-SEI and SEM-EDS) was performed to assess scale morphology, interfacial roughening and for elemental analysis of the scale-steel interface.

The following general observations were made: The effects of the different fluxes (industrial and synthetic) were similar. Visual examination of the samples after reheating and descaling showed that all synthetic fluxes gave better descaling (than for uncontaminated samples), and especially so the flux SMF1.

Even a small coverage of mould flux contaminant on steel surface was found to facilitate descaling. However, for average coverage below 20 μm the mould flux effect was found to break down, and descaling was difficult.

Figure 4.1 illustrates the scale layers on the steel after high temperature oxidation.

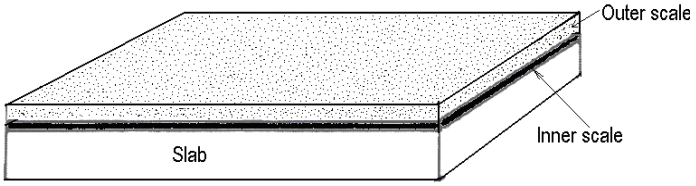

FIGURE 4.1: Sketch of the scale layers formed on the surface of the reheated sample.

Results of XRF analysis of the outer scale removed from the samples are presented in table 4.2. These samples were obtained after reheating of uncontaminated samples and contaminated samples (with mould flux type RF1) at 1250°C, 4% O_2 for 2 hours.

TABLE 4.2: XRF- analysis of the removed outer scale after cooling the sample in a nitrogen-flushed box following reheating at 1250°C for 2h, with 4% O_2 in gas.

%	S6	S7	S10	S11	S12
	Flux RF1	No Flux	Flux RF1	Flux RF1	No Flux
Cr_2O_3	12.820	7.500	9.730	10.850	12.510
Fe_2O_3	76.520	85.980	81.700	77.880	78.990
NiO	5.470	3.640	4.520	4.450	5.020
SiO_2	1.060	0.237	0.807	1.860	1.030
CaO	0.702	0.002	0.468	1.690	0.084
MnO	2.06	1.96	1.64	1.94	1.66
MgO	0.038	0.022	0.023	0.047	0.021
Na_2O	0.232	0.099	0.167	0.318	0.080
K_2O	-	-	0.004	0.011	0.005
Al_2O_3	0.142	0.005	0.363	0.254	0.113
V_2O_5	0.12	0.013	0.12	0.12	0.012
MoO_3	0.30	0.01	0.22	0.33	-
TiO_2	0.03	0.02	0.02	0.03	0.01
P_2O_5	0.45	0.43	0.2	0.15	0.36
SO_3	0.03	0.03	0.03	0.08	0.09
CuO	0.05	0.06	0.03	0.05	0.06
Total	100	100	100	100	100

The thicknesses of the removed outer scale on sample S6 (contaminated sample) and S7 (uncontaminated sample), both reheated for two hours, were measured after the outer scales were detached from the upper surfaces of these samples. The outer scale removed from S7 (uncontaminated) was 0.2mm thick and the scale remaining on the sample was 0.44mm thick, giving a total scale thickness of 0.64 mm on the upper sample surface after reheating. For sample S6 (contaminated), the removed scale was

about 0.4mm thick, and the scale remaining on this sample was around 0.1mm thick, for a total scale thickness of 0.5 mm. This slight decrease in the extent of oxidation for samples with mould flux was also found for different reheating conditions, as discussed later in this chapter. The difference in behaviour between contaminated and uncontaminated slabs was also visible for short reheating times. For contaminated samples reheated for 2 hours with 3% free oxygen at 1250°C, some parts of the steel surface were found to be unoxidized, indicating a protective effect of the mould flux.

Similar XRF analyses were performed on the outer scales on the steel after reheating contaminated and uncontaminated samples, for mould flux type 832 and synthetic mould fluxes SMF1, SMF2 and SMF3. The results are presented in table 4.3. Samples RP2 and RP3 were reheated at 1250°C, for 3h, 4% O_2 in gas (the latter covered with flux type 832; C_f = 0.015g/cm^2). Samples RP5 and RP8 (the latter covered with flux type 832; C_f = 0.015g/cm^2) were reheated at 1280°C, for 6h, 4% O_2 in gas. Samples RTS99 (covered with synthetic flux containing 20% Na_2O), RTS 100 (synthetic flux with 20% CaF_2) and RTS122 (synthetic flux with 50% CaO-50% SiO_2) were reheated at 1280°C, for 5h, 4%O_2 in gas.

TABLE 4.3: XRF analyses of outer scale after reheating, for uncontaminated samples, and samples contaminated with industrial and synthetic mould fluxes. See text for detail of reheating conditions.

	RP2	**RP3**	**RP5**	**RP8**	**RTS99**	**RTS 100**	**RTS 122**
	No flux	Flux Type 832	No flux	Flux type 832	Flux SMF2	Flux SMF1	Flux SMF3
SiO_2	0.33	1.63	0.32	1.62	0.87	2.50	3.67
TiO_2	<0.01	0.02	0.01	0.03	0.01	0.04	0.02
Al_2O_3	<0.01	0.19	0.03	0.19	0.09	<0.01	0.09
Fe_2O_3	75.40	72.76	75.99	69.92	77.49	66.53	70.04
MnO	1.98	1.96	1.68	1.71	1.47	1.73	1.70
MgO	1.18	<0.01	<0.01	<0.01	<0.01	<0.01	<0.01
CaO	0.50	2.08	0.26	2.70	1.84	4.29	3.37
Na_2O	<0.01	<0.01	<0.01	<0.01	<0.01	<0.01	<0.01
K_2O	0.02	0.01	<0.01	<0.01	0.03	<0.01	<0.01
P_2O_5	0.88	0.75	0.74	0.94	0.78	0.93	0.66
Cr_2O_3	12.77	14.79	15.92	17.27	11.91	18.43	13.86
NiO	4.90	5.06	4.72	4.88	5.07	4.82	5.93
V_2O_5	0.10	0.11	0.12	0.15	0.16	0.13	0.12
SO_3	1.45	0.23	0.09	0.44	0.13	0.12	0.17
MoO_3	0.36	0.30	0.06	0.02	0.03	0.41	0.31
Cl	0.07	0.01	<0.01	0.03	0.03	0.03	0.01
CuO	0.06	0.07	0.07	0.07	0.07	0.04	0.07
Total	100	100	100	100	100	100	100

The XRF results in table 4.3 show that, for similar reheating conditions, there is little difference between the composition of the outer scale on samples with or without mould flux residues, apart from the presence (as expected) of CaO and SiO_2 in the scale of samples which had been contaminated with mould flux. The bar graphs in figure 4.2 and figure 4.3 illustrate the slight differences in mass percentage observed in tables 4.2 and 4.3 between the components of the removed outer scales on uncontaminated and contaminated samples.

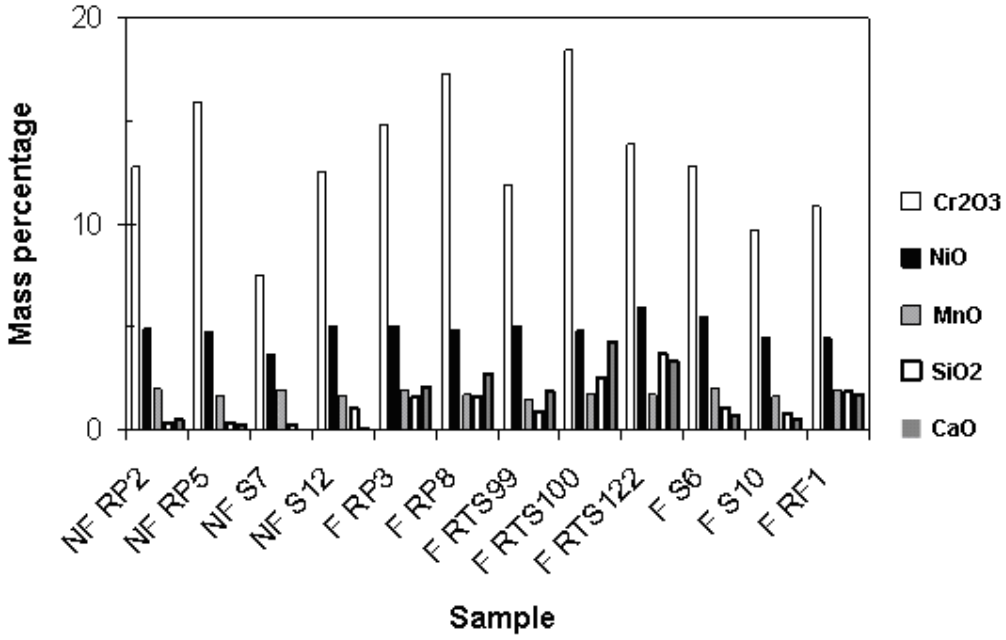

FIGURE 4.2: Mass percentage of Cr_2O_3, NiO, MnO, SiO_2 and CaO components of the removed outer scales on uncontaminated and contaminated samples

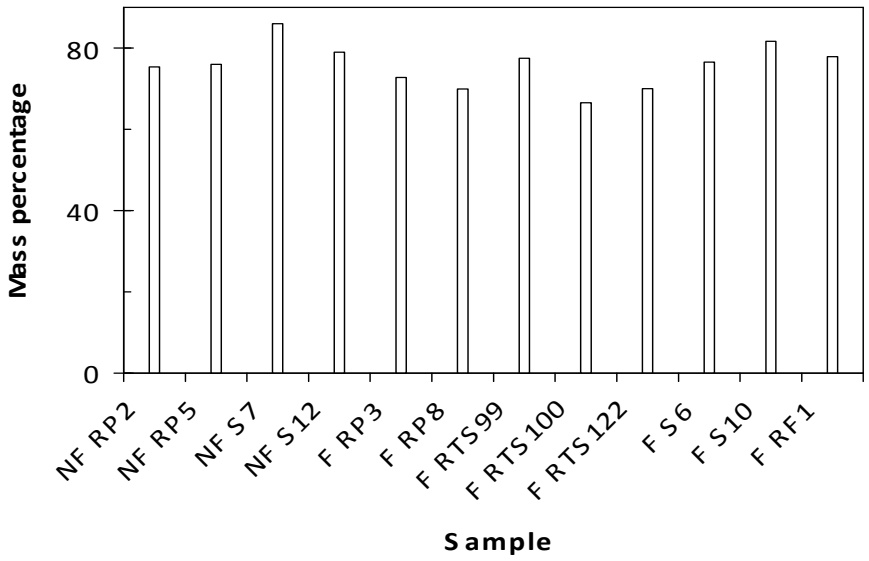

FIGURE 4.3: Mass percentage of Fe_2O_3 of the removed outer scales on uncontaminated and contaminated samples

Using SEM-EDS microanalyses on contaminated samples, residual mould flux was found at the steel-scale interface (see section 4.2.2.3 for details) and at the interface of two scale layers, Platinum wire markers, that had been placed on the sample surface before reheating were located at the interface of the inner and outer scale layers - demonstrating that the outer scale grew by cation diffusion, and the inner scale by internal oxidation.

4.2 DISCUSSION OF THE REHEATING RESULTS

4.2.1 Introduction

In this section, XRD analysis of the outer and inner scale layers, SEM-BSE micrographs of reheated samples close to scale-steel interface, and SEM-EDS[1] results in the scales are presented and discussed. Scales thicknesses were also measured.

4.2.2 Scale Characterisation

4.2.2.1 Thickness of Scales

Typical scale thicknesses after reheating in 3%O_2, for 6h at 1280°C, followed by descaling of samples D20 and D21 (SP =13.94 MPa, U = 26.22 l/m^2, I = 1.45 N/mm^2), were as follows:

[1] The light elements carbon, oxygen and fluorine were not analysed by SEM-EDS.

For the uncontaminated samples the removed scale was 875 µm thick, and the residual scale thickness was 580 µm, giving a total scale thickness after reheating of 1.455 mm. For the contaminated samples the removed scale was 1100 µm thick, and the residual scale thickness was 30 µm (in only a few places on the metal substrate; many places had essentially no residual scale), so up to 1.130 mm of scale had formed during reheating. This confirms the effect of mould flux residues to decrease oxidation slightly. Measurement of the decrease in sample thickness after reheating confirmed that the presence of mould flux causes a slight decrease in the scale growth rate.

From XRD analysis (see Figures 4.4 and 4.5) of the removed scales from the contaminated and the non contaminated samples, in both scale there were spinels (chromite) in the inner scales, and magnetite and haematite in the outer scale.

The outer scales were similar in phase composition (in line with the similarity in chemical composition, as reported in Tables 4.2 and 4.3), but the inner surfaces of the removed scales were quite different: metal phase (Ni-enriched tendrils, denoted by Fe γ in Figure 4.4) was found in the inner scale of the uncontaminated samples only, and not in the contaminated samples. This agrees with the microscopic appearance of scale cross-sections, as presented in the next section.

XRD-spectra of the underlying metal surface (with residual scale) and of the bottom of the removed scale showed in addition to the austenite phase, the presence a spinel phase on the non contaminated steel.

For the contaminated steel, XRD-spectra of the underlying metal and the bottom of the removed scale showed austenite and eskolaite (Cr_2O_3) (labelled "Fe_2O_3" in figure 4.4) and spinel (Figures in appendix 3).

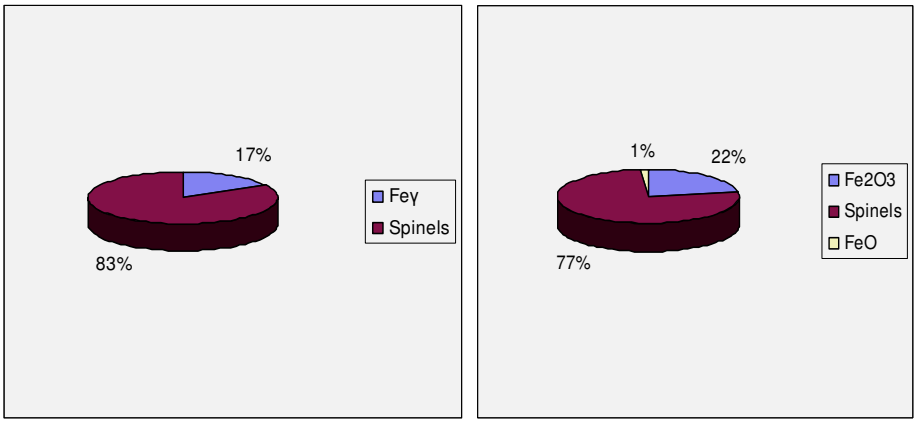

FIGURE 4.4: Phase compositions, from XRD, of the inner surface of the removed scale for the uncontaminated (left) and contaminated samples (right).

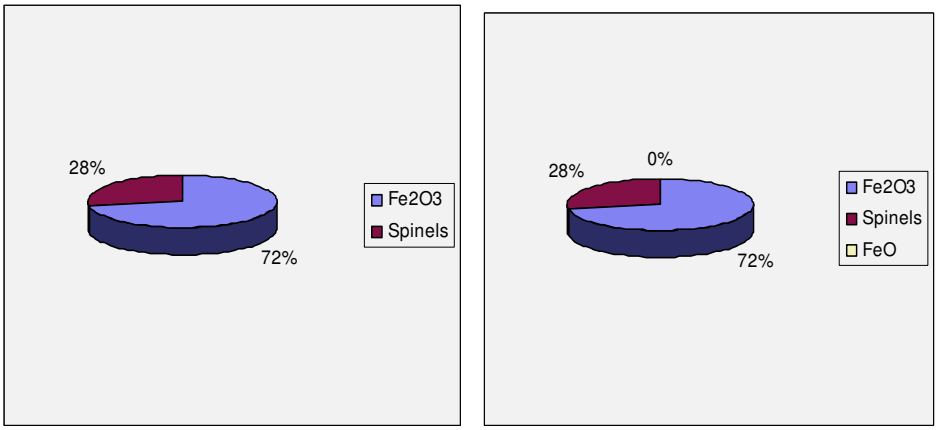

FIGURE 4.5: Phase compositions, from XRD, of the outer surface of the removed scale for the uncontaminated (left) and contaminated samples (right).

4.2.2.2 Microanalyses: Uncontaminated Sample after Reheating

Figure 4.6 shows a micrograph of the structure of the inner scale on an uncontaminated sample; the scale is towards the upper part of the image and the metal substrate towards the bottom part. Close to the scale-metal interface the scale mainly contained two phases: chromite (Fe-Cr spinel), originally formed along austenite grain boundaries by internal oxidation (darker phase), and metal tendrils formed by enrichment of the nobler metal (Ni) enrichment at the interface scale-metal substrate (bright phase). The composition of these two phases varies somewhat from the inner scale to the outer scale, but the metallic phase (tendrils) is always rich in Fe and Ni and the oxide phase (chromite) is rich in Fe and Cr.

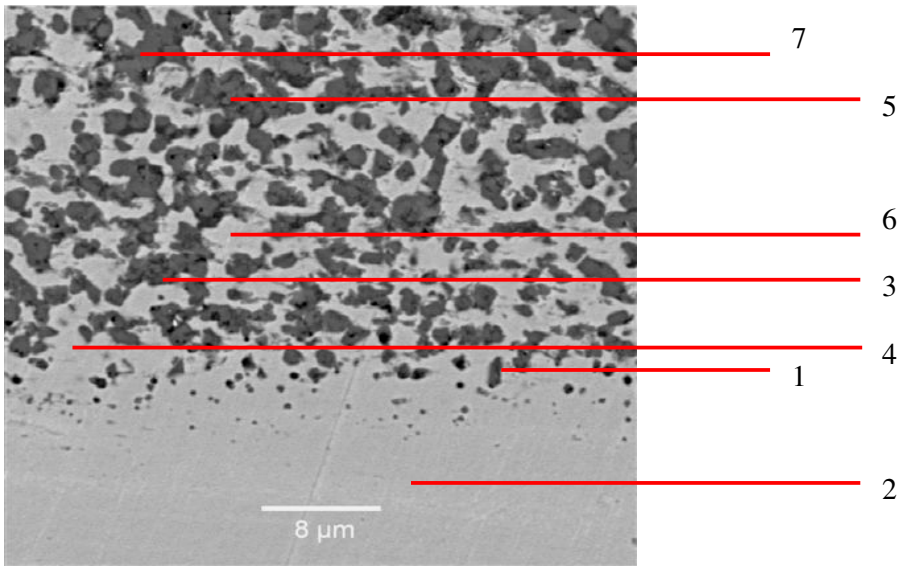

FIGURE 4.6: SEM backscattered electron micrograph of reheated sample – scale-steel interface; sample RP5 (no flux, 1280ºC, 4% O_2, 6h); analyses in Table 4.4.

TABLE 4.4: Average composition of different scale phases after reheating of uncontaminated sample (95% confidence intervals given). Sample RP5, 1280°C, 4%O_2, and 6h.

	Cr	Ni	Fe	Si	Ca	V	Mn
Point 2	4.1±1.7	14±4	81±2.5	0.2±0.12	0.1±0.14	0.02±0.14	0.21±0.3
Oxide 1	29.8±4.5	4.4±1.6	49.7±3.5	5.2±1.8	0.04±0.06	0.1±0.04	10.6±2.8
Oxide 3	52±5	1.4±1.4	38.4±6	1.4±1.3	0.12±0.15	0.8±0.7	5.9±3
Oxide 5	57.1±4.3	0.5±0.4	37.2±6	1.3±1.1	0.08±0.14	0.54±0.3	3.3±2.3
Tendril 4	8.5±4.9	11.74±2	78.9±3.5	0.33±0.3	0.06±0.1	0.12±0.2	0.42±0.5
Tendril 6	4.7±2.4	14.4±2.2	80±2.7	0.3±0.3	0.0±0.0	0.12±0.15	0.6±0.6
Point 7	11.9±3.4	0.9±0.4	82±6.8	2.55±5.4	0.08±0.1	0.16±0.2	2.4±1.5

4.2.2.3 Microanalyses: Contaminated Samples after Reheating

Figure 4.7 gives a micrograph of the inner scale on a sample which had been contaminated with mould flux before reheating. Comparison with Figure 4.6 (uncontaminated sample) shows the major difference to be the absence of Ni-enriched tendrils on the contaminated surface.

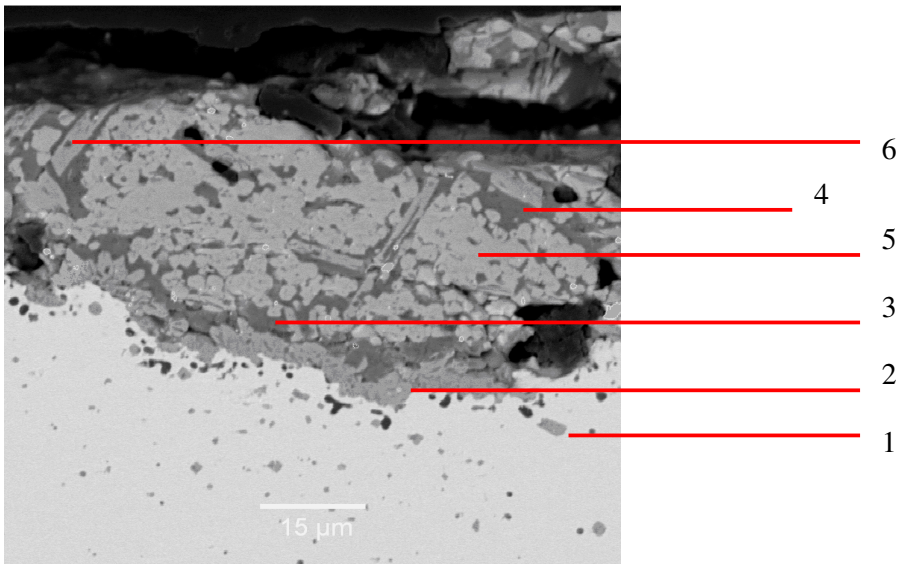

FIGURE 4.7: SEM backscattered electron micrograph of reheated slab sample – scale-steel interface; sample RP8 (flux type 832, 1280°C, 4%O_2, 6h); analyses in Table 4.5.

TABLE 4.5: Average composition of different scale phases after reheating of contaminated sample (95% confidence intervals given). Sample RP8, flux type 832, 1280°C, 4%O_2, C_f = 0.015g/cm^2, 6h

	Cr	Ni	Fe	Si	Ca	Na	Mn
Internal Oxide 1	56.36±2.9	1.28±0.6	13.56±6.4	0.18±0.1	0.18±0.05	0.0±0.0	26.87±4.1
Interface 2	90.18±4.3	0.14±0.2	7.84±4.7	0.32±0.1	0.5±0.08	0.02±0.5	0.6±0.15
Flux 3	7.75±8.54	0.45±0.24	3.68±1.88	32.95±2	54.53±8	0.15±0.08	0.35±0.26
Flux 4	9.9±7.89	1.7±0.31	6.5±2.5	30.6±3	50.2±8	0.1±0.1	0.8±0.2
Oxide 5	40.13±0.6	16.1±0.5	38.38±0.5	0.33±0.3	0.63±0.24	1.5±0.3	4.35±0.5
Oxide 6	72.3±4.4	0.83±0.51	24.95±5.3	0.58±0.77	0.8±0.63	0.13±0.21	0.35±0.33

The internal oxide (point 1 in Figure 4.7) was similar in composition to that in the uncontaminated sample. However, other phases are present in the contaminated sample which are not found on the uncontaminated sample:

An oxide layer at the scale-steel interface – nearly pure chromium oxide (point 2).

Mould flux residues (points 3 and 4), with dissolved Cr, Ni and Fe; the absence of Na in the remnant flux is probably due to the volatilisation.

Mixed Ni-Cr-Fe-Mn oxide (point 5): Dominant mid-grey phase away from interface; apparently steel of which the oxidation was enhanced by mould flux.

Needle like crystals within the scale (point 6): These are rich in Cr (they are probably chromite, but with a higher Cr content than the spinel in the uncontaminated sample)

Similar scale structures were found for samples contaminated with synthetic mould fluxes, as detailed below in Tables 4.6, 4.7 and 4.8 and Figures 4.8, 4.9 and 4.10.

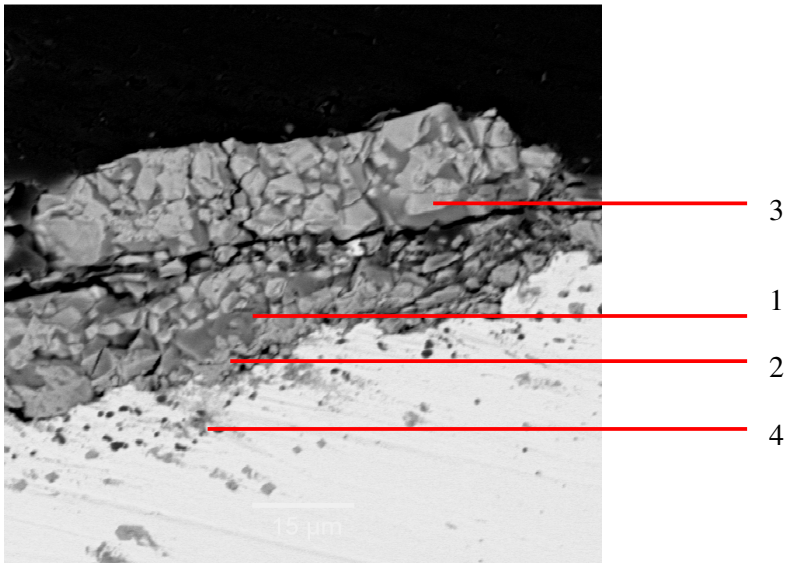

Figure 4.8: SEM backscattered electron micrograph of reheated contaminated sample – scale-steel interface; sample RTS9 (synthetic flux SMF2 with 20% Na_2O); analyses in Table 4.6.

TABLE 4.6: Average composition of different scale phases after reheating of contaminated sample (95% confidence intervals given), Sample RTS9, 20% Na_2O synthetic flux SMF2, 1280°C, 4%O_2, 6h, C_f = 0.016g/cm^2.

	Cr	**Ni**	**Fe**	**Si**	**Ca**	**Na**	**Mn**
Internal oxide 4	52.53±1.5	1.93±0.74	18.78±2.3	1.35±1.8	0.3±0.2	0.05±0.01	23.88±3
Interface 2	86.98±4.5	0.93±0.8	8.8±2.4	0.78±0.8	0.85±0.64	0.2±0.19	0.28±0.28
Oxide 3	49.5±1.9	18.23±1.2	28.4±1.39	0.48±0.17	0.55±0.24	0.28±0.47	2.45±0.89
Flux 1	9.49±5.9	1.53±2	18.2±2.12	42.65±6	20.73±1.7	5.35±0.7	0.63±0.7

The scale on the sample contaminated with the Na_2O-containing synthetic flux (Table 4.6) contained the following phases:

The internal oxide (point 4) was similar in composition to that in the uncontaminated and other contaminated samples.

Nearly pure chromium oxide was found at the scale-steel interface (point 2), as for the sample contaminated with the commercial flux (Figure 4.7 and Table 4.5).

Similarly, the mould flux remnant (point 1) had lowered Na, and contained dissolved Cr, Ni and Fe, and the dominant mid-grey oxide away from interface (point 3) was a mixed Cr-Fe-Ni-Mn oxide.

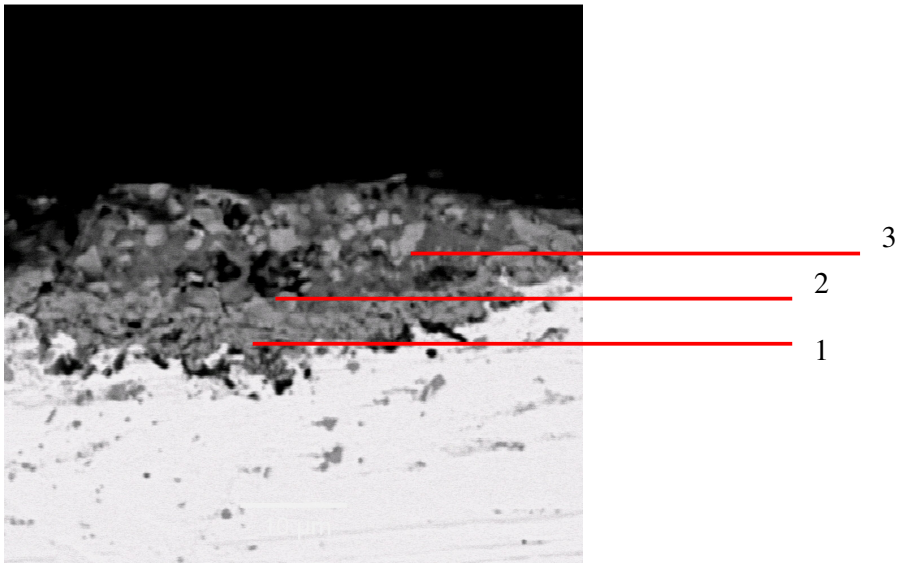

FIGURE 4.9: SEM backscattered electron micrograph of reheated sample – scale-steel interface; sample RST 10 (synthetic flux SMF1 with 20% CaF_2); analyses in Table 4.7.

TABLE 4.7: Average composition of different scale phases after reheating contaminated sample (95% confidence intervals given). Sample RST10, 20% CaF_2 synthetic SMF1, 1280°C, 4%O_2, 6h, $C_f = 0.017 g/cm^2$

	Cr	Ni	Fe	Si	Ca	Na	Mn
Interface 1	91.28±3.8	0.46±0.5	5.04±3.2	0.72±0.6	0.96±0.6	0.24±0.3	0.86±0.6
Flux 2	28.2±4	0.33±0.2	13.5±2.6	22.6±1.5	34.2±1.3	0.28±0.28	0.73±0.6
Oxide 3	42.1±70	5.45±2	40±6.3	1.2±0.6	2.63±0.7	0.03±0.05	8.3±20

The scale on the sample contaiminated with the CaF_2-containing synthetic mould flux (Figure 4.9 and Table 4.7) had three major phases:

Nearly pure Cr oxide at the scale-steel interface (point 1).

Mould flux residue, containing dissolved Cr, Fe and possibly Ni (point 2).

Cr-Fe-Mn-Ni mixed oxide away from the interface (point 3).

The scale on the sample contaiminated with the CaO-SiO_2 synthetic mould flux (Figure 4.10 and Table 4.8) had similar phases:

Internal oxidation product (point 4): Cr-Fe-Mn oxide, as in the other samples.

Nearly pure Cr oxide at the scale-steel interface (point 1).

Mould flux residue, containing dissolved Cr, Fe and Ni (point 2).

Fe-Mn-Ni mixed oxide away from the interface (point 3).

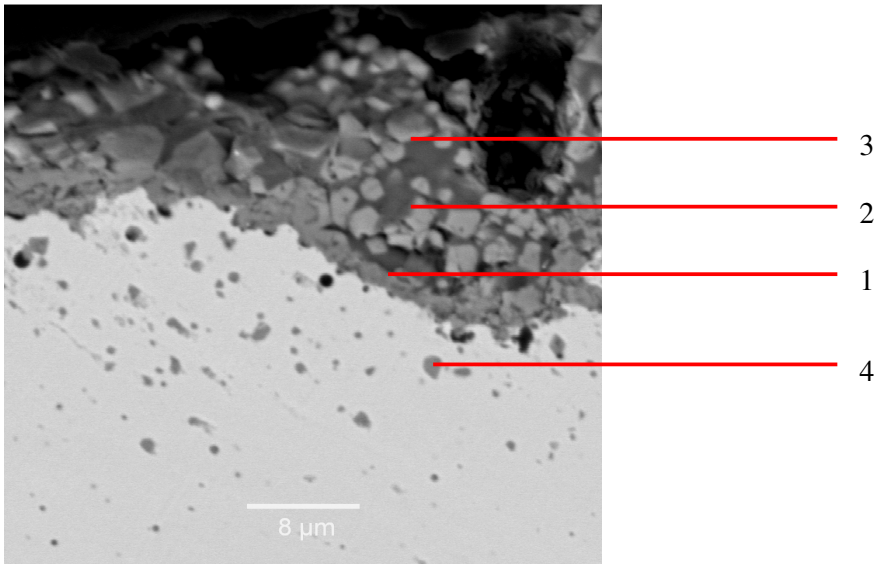

FIGURE 4.10: SEM backscattered electron micrograph of reheated sample – scale-steel interface; sample RTS 12 (50%CaO-50%SiO_2 synthetic mould flux SMF3); analyses in Table 4.8.

TABLE 4.8: Average composition of different scale phases after reheating of contaminated samples (95% confidence intervals given). Sample RTS 12, 50%CaO-50%SiO_2 synthetic mould flux SMF3 (6h, 1280°C, 4%O_2, C_f = 0.016 g/cm^2).

	Cr	**Ni**	**Fe**	**Si**	**Ca**	**Na**	**Mn**
Internal oxide 4	57.73±4.1	0.93±0.6	9.53±3.5	0.35±0.6	0.73±0.2	0.4±0.5	28.93±3
Interface 1	89.83±4.2	0.5±1	5.1±2.5	1.03±1.6	1.63±0.8	0.2±0.34	1±1.34
Flux 2	13.75±8	3.75±1.97	15.68±1.4	29.8±4.9	35.83±4	0.1±0.2	0.8±0.89
Oxide 3	54.55±1.5	11.35±1.7	29.8±2.3	0.53±0.4	1.38±0.2	0.68±1.1	1.38±0.98

Figure 4.11 illustrates internal oxidation after reheating at 1280°C for 6 h with 4%O_2 in the gas phase. The micrographs are for an uncontaminated sample, a sample contaminated with industrial flux type 832, and a sample contaminated with synthetic flux SMF2. From these images, there appears to be a tendency for a greater depth of internal oxidation in the presence of the mould flux. However, this effect was not quantified in this work.

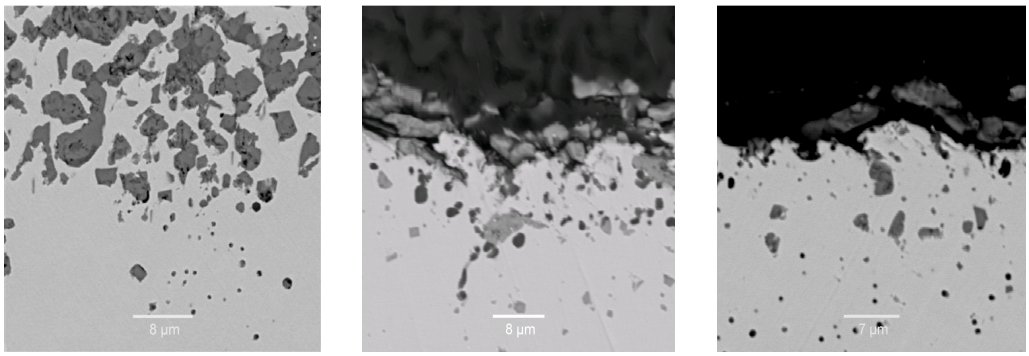

No Flux (RP5) Industrial flux (RP8) Synthetic flux (RST10)

FIGURE 4.11: Sample appearance (scale-steel interface) after reheating under similar conditions. Surface condition (from left to right): uncontaminated; contaminated with industrial flux (type 832); and contaminated with synthetic flux (SMF2). Backscattered electron images.

4.2.3 Summary of differences in scale structure

The difference in interfacial roughening (as distinct from tendril formation) between uncontaminated and contaminated samples was relatively small. In contaminated samples roughness at the interface generally appeared to be slightly greater than in the uncontaminated samples.

The difference in scale microstructure is illustrated by figure 4.12 and figure 4.13 below (scale is towards the upper part of the images and the metal substrate towards the lower part):

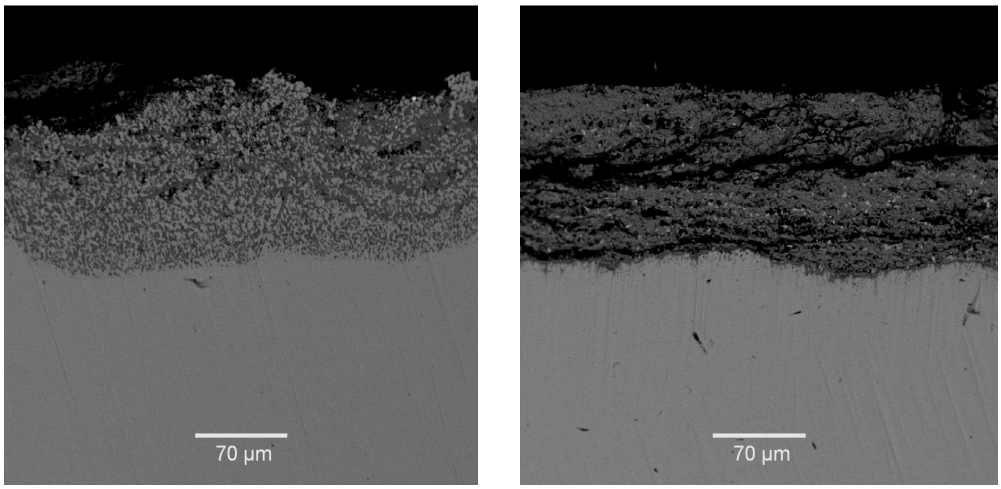

FIGURE 4.12: Difference in scale morphology for uncontaminated sample S7 (left) and contaminated sample S6 (right), after 4 hours reheating with 4 % free oxygen at 1250°C. Backscattered electron images.

The scales for contaminated and uncontaminated samples are very different, both in internal structure, and with respect to the compositions of the oxide phases. The absence of Ni-enriched tendrils in the scale of fluxed slab surfaces is a striking effect, with clear implications for descaling effectiveness. This effect apparently arises because mould flux contamination enhances the oxidation of nickel and chromium. Usually upon reheating nickel (being more noble than iron) accumulates in the remaining metal, while chromium (being less noble metal than iron) forms chromite by internal oxidation, at sites which include austenite grain boundaries. Both of these effects appear to be suppressed by the presence of mould flux on the sample surface: nickel in the scale is oxidised, and is not present in metal tendrils, and chromium oxide forms a continuous inner scale, between the mould flux remnants and the steel. In addition to the images shown in the previous section, further micrographs are given here to emphasise the differences.

For the uncontaminated samples, the inner scale exhibited scale entanglement with tendrils of unoxidized metal (see Figure 4.13), as expected from the high nickel

content of this steel. In Figure 4.13 the metal tendrils are visible as the lighter regions entwined with darker oxide (chromite). Close to the steel-metal interface these tendrils typically contained 5-9% chromium and 12-14% nickel (balance iron).

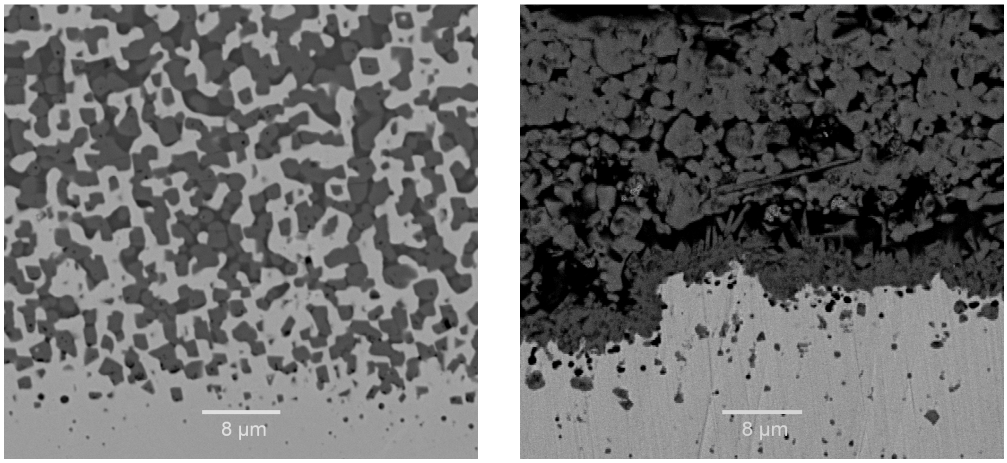

FIGURE 4.13: Appearance of the scale-steel interface on uncontaminated sample R3 (left) and contaminated sample R2 (right) after reheating at 1250°C, 4% O_2, 6 hours. Backscattered electron images.

In line with previous results (Pistorius *et al.*, 2003) narrow paths through the scale were found to be free of the nickel-enriched tendrils; these paths - corresponding to chromite in composition - follow the former austenite grain boundaries, and extend into the metal beyond the macroscopic scale-steel interface (see arrows in figure 4.14). These chromite paths should facilitate the descaling of non-contaminated samples to some extent.

For contaminated samples, close examination of the steel-scale interface did not reveal any oxide penetration into the steel, tendrils of unoxidised metal or the presence of the metal free paths-corresponding to chromite (see figures 4.13 and 4.14). In this case, however, there were longitudinal cracks (fissures) formed parallel to the surface (see figure 4.12). These would favour complete or partial descaling, depending on the location of the cracks close to or near the metal-scale interface. A complex structure can be seen at the scale-steel interface which contains needles, nodules, voids and discontinuities within the body of the scale (see figures 4.13 and

4.14). It is unclear whether these voids formed during reheating, or whether particles of scale were lost during sample preparation despite the precautions taken. Taniguchi (1985) claimed that the porosity or interfacial voids can bring the loss of adhesion and facilitate scale removal.

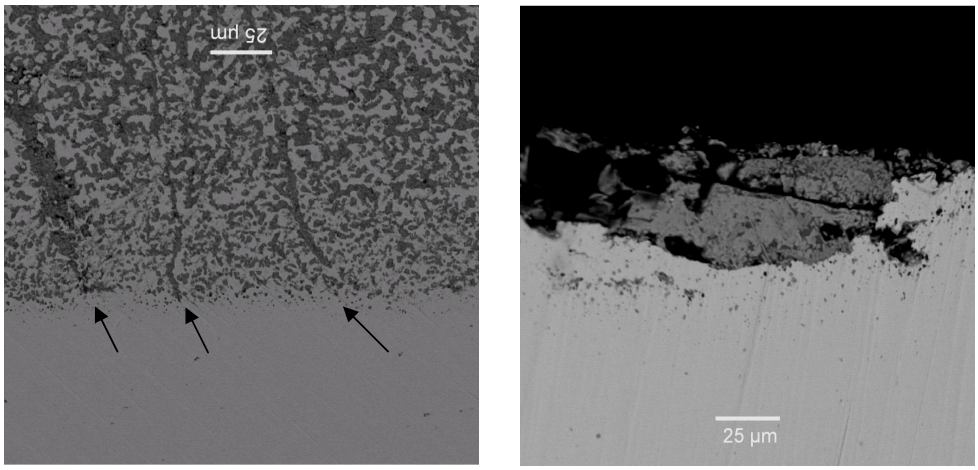

FIGURE 4.14: Interfacial microstructure of the uncontaminated side (left) and the contaminated side (right) of a plate sample (RP88) reheated at 1280°C, 4% O_2, 6 hours; after descaling (SP=13.94 MPa, U=26.22l/m^2; I=1.45N/mm^2, mould flux concentration on the contaminated side is C_f=0.011g/cm^2). Backscattered electron images.

For uncontaminated samples, the scale did not contain lateral or perpendicular cracks close to the metal substrate, which would presumably render the scale difficult to remove (figure 4.14). The inner scale appeared to be adherent as a result of entanglement and occlusion of metal particles in the scale. These metal particles (tendrils) were linked to form a network. The irregular metal/inner scale interface is expected to mechanically key the scale to the steel. There was also significant grain boundary oxide penetration. Thus, descaling should remove the outer scale and not the inner scale.

4.2.4 Analysis of the Removed scale for Chromium Oxidation State

The oxidising furnace atmosphere and presence of basic components (CaO and Na_2O) in the mould flux could lead to formation of the undesirable Cr (VI) species during

reheating of contaminated samples (Page and Loar, 2004). X-ray photo-electron spectroscopy was hence used to determine the oxidation state(s) of chromium in the scale.

XPS analysis was performed on both contaminated and uncontaminated samples. A mathematical curve fit procedure for the $Cr2P_{3/2}$ photoelectron peak was performed; peak positions that are associated with average binding energies of 573.94eV, 575.65eV and 577.02eV were identified. Based on comparison of these binding energies with standard spectra of various chromium species (NIST Database, 1989), it can be assumed that the lowest binding energy 573.94±0.95eV is associated with chromium (0) (metallic phase present at the interface), the binding energy 575.65±0.36 eV is associated with chromium (III) (in Cr_2O_3), and the binding energy 577.02±0.41eV is associated with chromium (III) (in spinel phases).

The presence of chromium (VI) would correspond to an average binding energy of 579.7±1.2 eV. This was not found after XPS deconvolution analysis; hence oxidation of chromium to the hexavalent state is not the origin of the differences in scale structure.

The XPS analyses (see Appendix 4) also confirmed that the amount of metallic phase in the removed scale was higher in the uncontaminated scale than in the contaminated scale (in line with the observed absence of metal tendrils in the contaminated scale).

4.3 DESCALING EXPERIMENTAL CONDITIONS AND RESULTS

Uncontaminated samples and samples contaminated with industrial mould fluxes (type 832, type 810 and type RF1) were reheated and descaled under similar conditions in order to assess the descaling effectiveness. After initial experiments, it was found that the samples were more sensitive to reheating parameters than descaling parameters (such as water flow rate, samples speed and descaling spray height). Further descaling was hence performed with different reheating parameters and constant speed and spray height. Descaling conditions were maintained close to those used in the industrial practice for the stainless steel type 304.

The experimental reheating conditions (using 3% and 4% free O_2) are shown in table 4.9.

TABLE 4.9: Reheating conditions for uncontaminated and contaminated samples which were hydraulically descaled

	% O_2	T[°C]	Time [h]	C_f [g/cm^2]	Mould flux type
D1	3	1300	5	0.023	RF1
D2	3	1300	5	0.022	832
D17	4	1280	6	0	–
D18	4	1280	6	0.011	810
D3	3	1300	5	0	–
D4	3	1300	5	0.035	RF1
D6	3	1280	5	0.015	RF1
D7	3	1280	4	0.016	810
D8	3	1280	6	0.015	832
D19	3	1280	6	0	–
D9	3	1280	5	0.021	RF1
D10	3	1250	6	0.015	RF1
D20	3	1280	6	0.015	810
D21	3	1280	6	0	–
D11	3	1250	2	0.008	RF1
D12	3	1250	6	0.011	RF1
D13	3	1250	6	0.017	832
D15	3	1280	6	0.015	810
D16	3	1280	6	0.016	832
RP22	4	1250	3	0	–
RP33	4	1250	3	0.015	832
RP44	4	1280	6	0.005	SMF3
RP55	4	1280	6	0	–
D177	3	1280	6	0	–
RP88	4	1280	6	0.011	RF1
RTS99	4	1280	5	0.017	SMF2
RTS1000	4	1280	5	0.017	SMF1

Descaling conditions are shown in table 4.10; in all cases the vertical nozzle height was 96 mm and the stock feed rate 0.8m/s.

Table 4.10**:** Descaling conditions, and visual appearance of samples after descaling. Runs of which the labels are shown in bold were for samples not coated with mould flux.

	Pr[KPa]	Qb[l/min]	SP[MPa]	U[l/m^2]	I[N/mm^2]	Appearance
D1	111.80	54.40	13.90	26.22	1.45	Descaled
D2	112.29	54.50	13.98	26.26	1.454	Descaled
D17	112.29	54.50	13.98	26.26	1.454	Residual scale
D18	112.29	54.50	13.98	26.26	1.454	Descaled
D3	174.95	64.07	19.83	30.87	2.036	Residual scale
D4	174.95	64.07	19.83	30.87	2.036	Descaled
D6	176.42	64.30	19.97	30.97	2.051	Descaled
D7	175.25	64.11	19.86	30.89	2.039	Descaled
D8	186.33	65.81	20.90	31.70	2.147	Descaled
D19	187.30	65.96	20.99	31.78	2.157	Residual scale
D9	171.62	63.56	19.52	30.62	2.004	Descaled
D10	174.56	64.01	19.80	30.84	2.033	Descaled
D20	111.80	54.43	13.94	26.22	1.45	Descaled
D21	111.80	54.43	13.94	26.22	1.45	Residual scale
D11	173.58	63.86	19.71	30.77	2.023	Descaled
D12	167.69	62.96	19.16	30.33	1.967	Descaled
D13	166.71	62.81	19.07	30.26	1.957	Descaled
D15	161.81	62.07	18.61	29.90	1.911	Descaled
D16	162.79	62.22	18.70	29.97	1.92	Descaled
RP22	111.80	54.43	13.94	26.22	1.45	Residual scale
RP33	111.80	54.43	13.94	26.22	1.45	Descaled
RP44	111.80	54.43	13.94	26.22	1.45	Partially descaled
RP55	111.80	54.43	13.94	26.22	1.45	Residual scale
D177	161.81	62.07	18.61	29.90	1.911	Residual scale
RP88	111.80	54.43	13.94	26.22	1.45	Descaled
RTS99	112.29	54.50	13.98	26.26	1.454	Descaled
RTS1000	111.80	54.43	13.94	26.22	1.45	Descaled

4.4 DISCUSSION OF THE DESCALING RESULTS

4.4.1 Thickness of the Residual Scale

According to the results of this investigation, austenite grain structure, the presence of Ni and Cr in the steel and mould flux contamination play major roles in the descaling behaviour of type 304 stainless steel.

The micrographs in Figure 4.15 show the difference in removed scale morphologies after descaling of the uncontaminated and contaminated samples under similar reheating and descaling conditions.

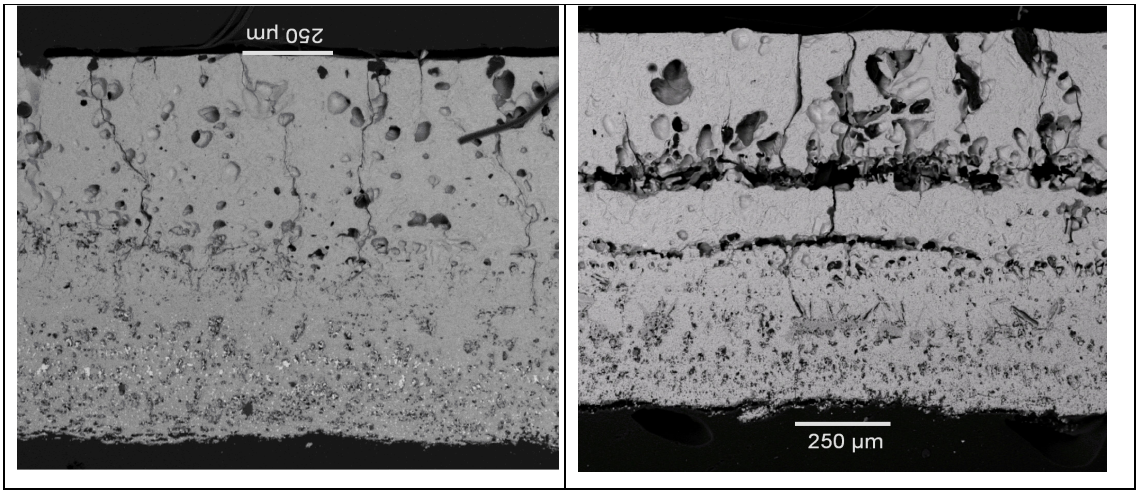

Figure 4.15: Cross-sections through scale removed from the uncontaminated sample D17 (left) and the contaminated sample RP88 (right; C_f=0.011 g/cm^2) after reheating (1280ºC, 4%O_2, 6h) and descaling (SP=13.94MPa, U=26.22/m^2, I=1.45N/mm^2). Backscattered electron images.

In the figure above the uncontaminated scale contains a layer of Ni-enriched tendrils in the inner scale (these are the bright spots in the lower part of the image), which confirms Ni enrichment at the scale-steel interface. The scale removed from the contaminated sample has no Ni-enriched metals tendrils in the inner scale. These observations are consistent with those presented in the previous sections.

Visual examination of the samples after reheating and descaling confirmed that the presence of mould fluxes promoted descaling (see Table 4.10).

4.4.2 Steel Surface after Descaling

Visual observation of the uncontaminated slab samples after descaling showed the presence of residual scale and a roughened surface. For the contaminated descaled steel, there were only a few places with residual scale, but the surfaces were mostly fully descaled. The microscopical appearance of cross-sections confirmed this (Figures 4.16 and 4.17), showing the adherent residual scale on the surface of the uncontaminated sample and the non-adherent residual scale on the surface of the contaminated sample. From measurements on cross-sections, the thickness of the residual scale on the uncontaminated steel was 440-550µm.

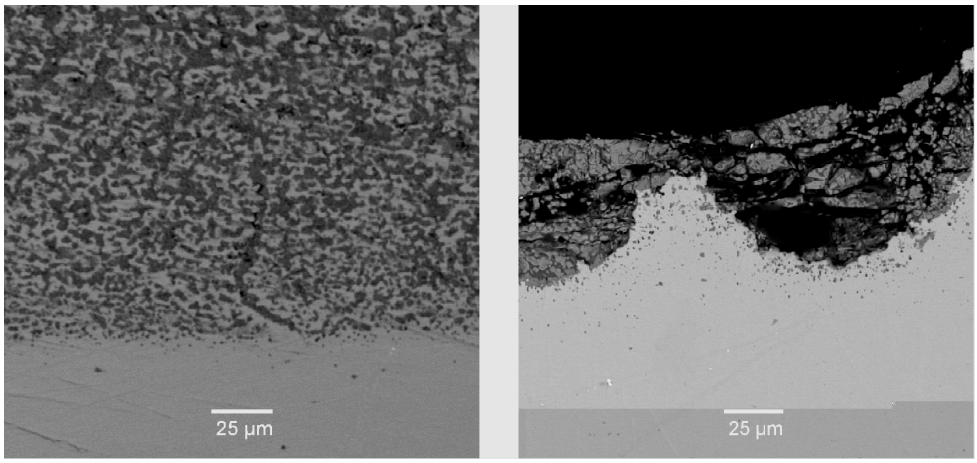

FIGURE 4.16: Difference in scale morphology of the residual scale after reheating and descaling of the uncontaminated (left) and contaminated (right); samples D16 and D177. Reheating and descaling conditions: 1280°C, 3% O_2, C_f = 0.016 g/cm^2 (on the contaminated sample), 6 h, SP = 18.61 MPa, U = 29.9 l/m^2, I = 1.91 N/mm^2. Backscattered electron images.

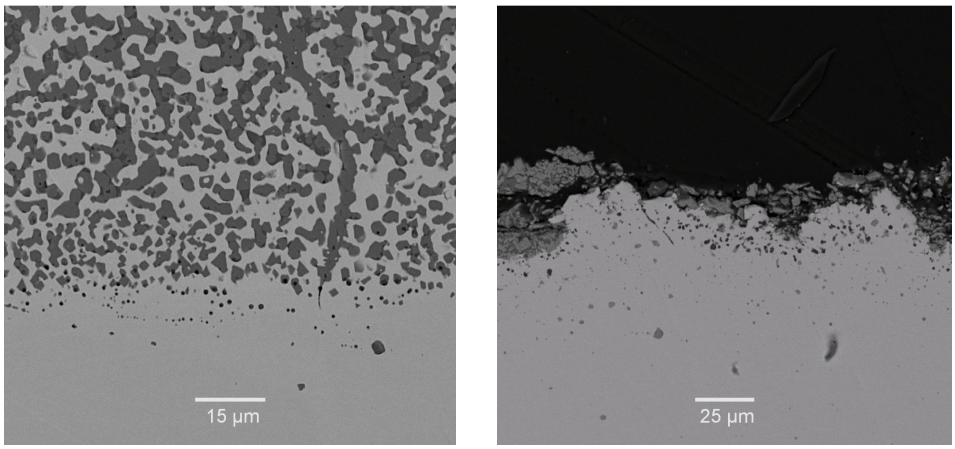

FIGURE 4.17: Residual scale on uncontaminated (left) and contaminated (right) plate surfaces of samples D19 and D8. Reheating and descaling conditions: 1280°C, 3% O_2, 6 h, C_f = 0.015 g/cm^2 (on the contaminated sample), I = 2.15 N/mm^2, U = 31.7 l/m^2. Backscattered electron images.

For contaminated samples, changes in temperature, time and the excess free oxygen (within the ranges studied) were found to have little effect on the oxidation rate and the descaling effectiveness, because descaling was always effective.

For uncontaminated samples, increases in temperature and longer reheating times were found to increase the extent of oxidation slightly, with poorer surface quality after descaling. A difference in the free oxygen content (3% and 4%) of the gas during reheating was found not to have major impact on the extent of oxidation.

The micrographs in figure 4.18 show the difference in the external appearance of the descaled surface for uncontaminated and contaminated samples (note that these are not cross-sections). The bright areas in the residual scale on the surface of the uncontaminated slab are Ni-enriched metal tendrils. These tendrils appear also in the inner part of the removed scale on the uncontaminated slab (see figure 4.15)

The bright areas on the contaminated slab surface are the chromium oxide layer (inner scale); EDX analysis gave a composition of 91.1% Cr; 6.2% Fe; 1.1% Si.

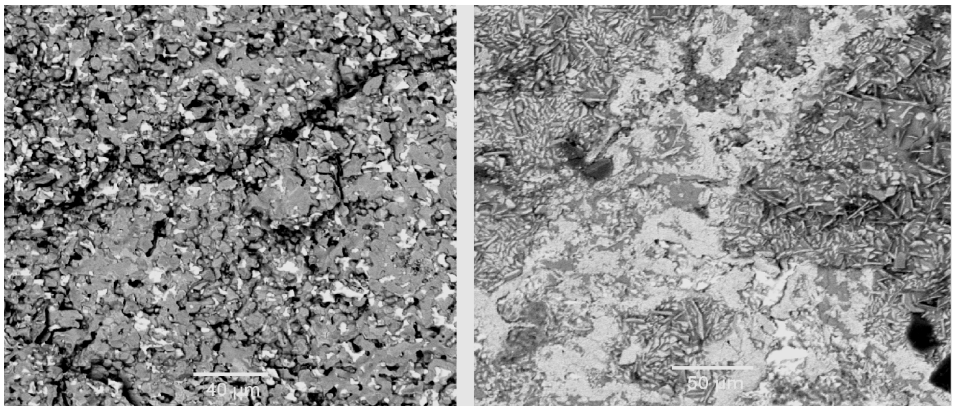

FIGURE 4.18: Difference in exterior appearance of descaled uncontaminated (left) and contaminated (right; C_f = 0.011 g/cm^2) slab samples D17 and D18; BSE images. Reheating and descaling conditions: 6 h, 4% O_2, 1280°C, SP = 13.98 MPa, U = 26.26 l/m^2, I = 1.45N/mm^2.

4.4.3 Effect of Descaling Variables

Descaling water system pressure, and hence impingement water flow rate, were varied in the first stage of this investigation and subsequently kept constant for the major part of the investigation, both to simulate industrial descaling conditions and also because it was found that descaling mainly depended on the reheating conditions rather than descaling conditions.

4.4.4 Mould Flux Effects on Descaling

In these experiments, the applied decarburised mould flux surface concentration varied between 0.005g/cm^2 and 0.035 g/cm^2, corresponding to average molten flux thicknesses of 19 µm to 135 µm on the steel surface. All mould flux surface concentrations explored during this project were found to give better descaling results, but the best results were found for mould flux surface concentration around 0.016 g/cm^2 or 60 µm of molten film on slab surface. Beyond 0.03 g/cm^2 or 115 µm, the slab surface was found to contain some black spots after descaling, possibly an excess of the unreacted mould flux on the steel surface. It should be noticed, in these experiments, below 0.008g/cm^2 (30 µm) of mould flux surface concentration it was difficult to obtain an even distribution of flux over the sample surface.

While all mould fluxes were found to give better descaling and steel surface quality, type 832 was found to be the best according to the descaled slab surface quality, followed by type RF1; descaled surface quality was assessed by visual examination of the samples, and SEM observation of both the metal-residual scale interface (cross-sectioned samples) and the exterior surface of the descaled samples.

4.5 PROPOSED MECHANISM BEHIND NICKEL OXIDATION

The direct cause of the much improved descaling for samples contaminated with mould flux is the disappearance of Ni-enriched metal tendrils. Clearly, the presence of mould flux promotes oxidation of nickel, and so avoids tendril formation. This effect does not depend on the details of the mould flux composition – the effect was found for industrial and synthetic mould fluxes, with and without CaF_2 and Na_2O. The underlying effect appears to be that NiO can dissolve in the mould flux, and that this favours nickel oxidation. There are limited data on this, but Lee *et al*. (2002) have summarised available data on the nickel oxide capacity of CaO-SiO_2-FeO slags. They propose that NiO dissolves in the slag through the oxidation reaction

$$Ni + 0.5\ O_2 + O^{2-} = NiO_2^{2-}$$

In this expression, O^{2-} anions provided by the slag (mould flux) react with the nickel oxidation products to form nickel oxide anions (NiO_2^{2-}) which dissolve in the mould

flux; the presence of iron oxide in the flux (which develops during scale growth) also enhances dissolution of nickel oxide (Lee *et al.*, 2002).

According to this mechanism, the beneficial effect of the mould flux would depend on its basicity (although the effect is not particularly strong – the nickel oxide capacity of C_2S-saturated slag is only 3 times that of lower-basicity slag with X_{CaO}/X_{SiO_2} = 0.5 to 0.7 [ibid.]).

Chapter 5: CONCLUSIONS AND RECOMMENDATIONS

Mould flux residues strongly change the nature of the inner scale (due to enhanced oxidation of nickel). The change in the nature of the scale-steel interface was found to enhance the descaling of the contaminated slabs.

For all contaminated samples, visual descaling effectiveness was approximately 100%.

For uncontaminated samples, visual descaling effectiveness was at best approximately 40% at 1300°C; 3% free O_2; 5 h reheating; I=2N/mm^2.

Mould flux type 832 (low CaO/SiO_2 ratio, but high Na_2O and CaF_2 content) was found to give the best descaling effectiveness and steel surface quality amongst the three industrial mould fluxes used for this investigation. Of the three synthetic mould fluxes used, it was found that mould flux SMF2 (20% CaF_2,40% CaO and 40% SiO_2) gave better descaling and better slab surface quality, similar to that obtained with mould flux type 832.

The remnant scale on the reheated samples after cooling of the contaminated sample in nitrogen box was very thin and the scale did not cover the entire surface.

For the contaminated samples it was found that descaling efficiency mostly depended on the reheating parameters (especially the presence mould flux on the steel surface) rather than the descaling parameters. For surfaces dosed with mould flux, it appears that the impact pressure could be reduced in industry without compromising descaling efficiency.

These results suggest future work on the effect of mould flux on scale adhesion to reheated slabs of other grades of stainless-steels and especially for nickel-bearing stainless steels. For example, dosing mould flux onto surfaces covered with nickel-enriched metal tendrils should destroy these tendrils; it would be interesting to test this possibility, and whether basicity does have the expected effect. The flux melting point would also be of important: binary $CaO-SiO_2$ mixtures are not molten at reheating temperatures, but the presence of FeO (and even Fe_2O_3) decreases the melting point considerably.